Geochemistry Geophysics Geosystems G3

Article
Volume 13, Number 3
23 March 2012
Q03020, doi:10.1029/2011GC004024
ISSN: 1525-2027

Published by AGU and the Geochemical Society

Dynamics of slab detachment

T. Duretz
ISTEP, UMR 7193, UPMC Paris 06, CNRS, F-75005 Paris, France (thibault.duretz@upmc.fr)

Institute of Geophysics, Department of Earth Sciences, ETH Zurich, CH-8092 Zurich, Switzerland

S. M. Schmalholz
Institute of Geology and Palaeontology, University of Lausanne, CH-1015 Lausanne, Switzerland

T. V. Gerya
Institute of Geophysics, Department of Earth Sciences, ETH Zurich, CH-8092 Zurich, Switzerland

[1] We investigate the dynamics of slab detachment around the detachment zone and evaluate the amount of time necessary for slabs to detach. The study combines results of two-dimensional (2D) state-of-the-art thermomechanical numerical simulations and a 1D analytical solution for viscous necking under gravity. We show that the dominant deformation mechanism during slab detachment is viscous necking, independent of the depth of slab detachment. When the slab dip is moderate (35–70°), slab detachment is partly affected by localized simple shearing in the colder parts of the slab. Brittle fracturing (breaking) plays a minor role during slab detachment. Our 2D thermomechanical models indicate that the duration of slab detachment, quantified from the onset of slab thinning until the actual detachment (i.e. vanishing of slab-pull force), is relatively short (<5 Ma) and can occur in less than 0.5 Ma. No clear correlation between the depth and the duration of slab detachment was observed. The simulations suggest that even deep slab detachment (>250 km) can occur within a short time interval (<1 Ma) which has implications for geodynamic interpretations using slab detachment as explanation for processes such as melting, exhumation or surface uplift. The thinning of the slab during detachment, observed in 2D simulations, agrees well with predictions from a 1D analytical solution indicating that the 1D solution captures the first-order features of the detachment process. We also evaluate the impact of shear heating on the duration of slab detachment. The predictions of a simple semi-analytical solution, based on dimensionless parameters, agree well with our and previously published results.

Components: 9500 words, 8 figures, 3 tables.

Keywords: necking; shear heating; shearing; slab breakoff; slab deformation; slab detachment.

Index Terms: 8120 Tectonophysics: Dynamics of lithosphere and mantle: general (1213); 8150 Tectonophysics: Plate boundary: general (3040); 8162 Tectonophysics: Rheology: mantle (8033).

Received 28 December 2011; **Revised** 20 February 2012; **Accepted** 20 February 2012; **Published** 23 March 2012.

Duretz, T., S. M. Schmalholz, and T. V. Gerya (2012), Dynamics of slab detachment, *Geochem. Geophys. Geosyst.*, *13*, Q03020, doi:10.1029/2011GC004024.

1. Introduction

[2] In the last decades, slab detachment has become a popular geodynamic research topic in both the geological and geophysical communities. This convergent margin process involves the detachment of a portion of the slab during ongoing subduction. The idea of slab detachment was born from the interpretation of geophysical observations and was employed to explain seismicity patterns within the subducting slabs [*Isacks and Molnar*, 1969; *Chatelain et al.*, 1993; *Chen and Brudzinski*, 2001; *Kundu and Gahalaut*, 2011]. The slab detachment model further gained popularity with the development of seismic tomography and the detection of slab remnants within the Earth's mantle [*Wortel and Spakman*, 1992; *Widiyantoro and van der Hilst*, 1996; *van der Meer et al.*, 2010; *Rogers et al.*, 2002; *Levin et al.*, 2002; *Schmandt and Humphreys*, 2011; *Zor*, 2008] and especially underneath orogens [*Lippitsch et al.*, 2003; *Martin and Wenzel*, 2006; *Replumaz et al.*, 2010].

[3] It is commonly accepted that slab detachment results from the development of extensional stresses within the downgoing plate. Subduction slowdown is considered to drive this stress build up [*Li et al.*, 2002] and is associated to the subduction of ridges or buoyant continental material. Two major consequences of slab detachment can be distinguished: (1) a partial or complete loss of the slab pull force and (2) the inflow of hot asthenosphere at the location of the detachment. The first consequence is commonly used in the explanation of tectonic processes such as exhumation of high pressure rocks [*Andersen et al.*, 1991; *Babist et al.*, 2006; *Xu et al.*, 2010], variations in surface uplift rates [*Rogers et al.*, 2002; *Morley and Back*, 2008] and in the sedimentary record [*Mugnier and Huyghe*, 2006], orogenic extension [*Zeck*, 1996], or rapid changes in plate motions [*Austermann et al.*, 2011]. The second consequence is usually considered as an efficient mechanism to advect heat at lithospheric to sub crustal level [*van de Zedde and Wortel*, 2001], subsequently triggering partial melting and plutonism [*Davies and von Blanckenburg*, 1995; *Ferrari*, 2004; *Altunkaynak and Can Genç*, 2004]. It has also been proposed that the entrainment of continental material by detached slabs in the mantle may play a role in the long term processes of crustal recycling [*Hildebrand and Bowring*, 1999].

[4] Given the potential implications of slab detachment, it is important to better understand the dynamics of slab detachment. In particular, we investigate the first-order thermomechanical process eventually leading to slab detachment and also the duration of slab detachment. Moreover, since slab detachment involves lithospheric-scale strain localization, we investigate the effect of viscous heating on the dynamics of slab detachment.

[5] Whereas thermomechanical models enable to test the influence of a variety of complicated model geometries, boundary/initial conditions, or material rheology [*Duretz et al.*, 2011a], simple analytical models give fundamental insights into the dynamics of slab detachment [*Schmalholz*, 2011]. In this study, we analyze and compare results of one-dimensional (1D) analytical and 2D numerical models in order to better understand the mechanism of slab detachment. The results of 2D simulations are used to quantify the duration of slab detachment, i.e. the time interval between the onset of thinning of the slab and the actual detachment of the slab. We refer to this time interval as slab detachment duration. Moreover, we evaluate the influence of shear heating on the slab detachment duration using predictions of a 1D semi-analytical solution.

2. Conceptual Models of Slab Detachment

[6] The detachment of a slab is often simplified in graphics as being the result of either a sharp fracture [e.g., *Nolet*, 2009], a shear zone [e.g., *Sacks and Secor*, 1990], or thinning (necking) [e.g., *Sacks and Secor*, 1990]. These schematic detachment models inherently involve contrasting physical modes of slab deformation: tensile brittle failure (Figure 1a), extension along a simple shear zone (Figure 1b), and pure shear necking (Figure 1c). The tensile failure model conveys the idea that the slab behaves as an homogeneous fragile plate for the pressure and temperature conditions of subduction zones. This model implies geologically instantaneous suction of the asthenosphere within the slab's crack and is therefore very inclined to explain fast heat advection and melting events. The simple shear model [*Sacks and Secor*, 1990] requires localized shear deformation without explicitly suggesting any rheological behavior of the slab (either viscous, plastic or brittle). The slab necking [*Sacks and Secor*, 1990] implies that the slab deformation is accommodated by pure shear viscous or plastic deformation. In this model, the asthenosphere advection velocity is proportional to the thinning rate of the slab. The model of *Lister*

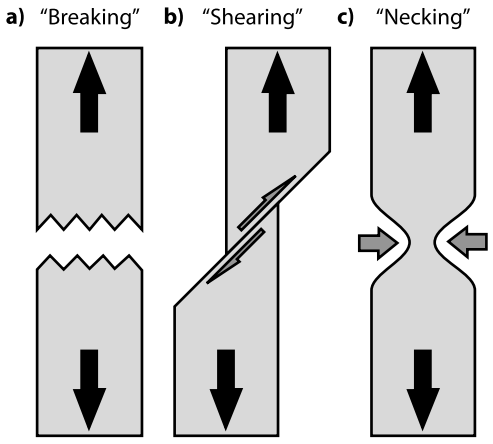

Figure 1. Typical conceptual illustrations of slab detachment. (a) Slab fracture (break-off) as the result of tensile failure (corresponding to a mode I fracture). (b) Simple shear model including the contributions of either plastic or viscous shear zones. (c) Necking model resulting from the extension of a (power law) viscous layer.

et al. [2008] combines necking (boudinage) and shear zones to explain the observed slab's morphology and the intraslab seismicity.

[7] On geological timescales, experimental and analytical studies suggest that olivine deforms by viscous deformation mechanisms such as grain-size sensitive and dislocation creep [*Hirth*, 2002; *Karato*, 2010; *Faul et al.*, 2011; *Rozel et al.*, 2011]. At low temperature (slab-like conditions), the deformation of olivine is expected to occur in the low-temperature plasticity regime (Peierls mechanism) [*Evans and Goetze*, 1979; *Kameyama et al.*, 1999; *Raterron et al.*, 2004; *Katayama and Karato*, 2008]. Consequently, a lithospheric-scale brittle (or breaking) behavior is not expected through entire slabs [*Replumaz et al.*, 2010]. However, the brittle slab break-off model is frequently visualized in sketches and graphics of slab detachment. We consider this break-off model as potentially misleading because it is often applied in geodynamic interpretations concerning both rheology and heat transfer. We consider the viscous shearing and necking models as more realistic thermomechanical models for the first-order deformation processes acting during slab detachment.

3. Insight From Mechanical and Thermomechanical Modeling

3.1. Methodology

[8] To study the dynamics of slab detachment, we use state-of-the-art 2D thermomechanical models of slab detachment [*Baumann et al.*, 2009; *Duretz et al.*, 2011a]. The simulations are performed with the thermomechanical code I2VIS (methodology and numerical analysis described by *Gerya and Yuen* [2003a] and *Duretz et al.* [2011b]). This numerical code solves the incompressible steady state momentum and heat conservation equations. Thermomechanical coupling is achieved by employing temperature-stress dependent viscosities and including viscous dissipation in the heat equation. The rheological model combines a diffusion-dislocation creep model with a Mohr-Coulomb stress limiter for each material. Exponential creep (Peierls mechanism of *Katayama and Karato* [2008]) can only be activated in the mantle. The effects of mineral phase transitions are taken into account by modifying the material properties according to their current pressure and temperature. The density and heat capacity of the mafic and ultramafic rocks are computed according to Gibbs energy minimization [*Connolly*, 2005]. The model assumes a pyrolitic mantle composition and a basaltic-gabbroic oceanic crust. The thermodynamic database is calculated for the chemical model $CaO\text{-}FeO\text{-}MgO\text{-}Al_2O_3\text{-}SiO_2$ [*Gerya et al.*, 2004; *Baumann et al.*, 2009]. The density of the continental crust and sediments evolve according to an equation of state [*Gerya and Yuen*, 2003b]. Our simulations are carried out in a 4000×1400 km size domain (Figure 2) and a maximum resolution of 1 km is achieved in the central part of the domain. Two 1300 km wide continents are separated by a 500 km wide oceanic basin and a weak zone is used to initiate the subduction. In order to generate a sufficient slab-pull force, the model is initially kinematically driven using convergence rates ranging between 1 and 10 cm/a. During this stage, the continents decouple from the lateral sides of the model domain, leaving the space for asthenosphere upwelling and the development of ridges. Once the oceanic lithosphere is subducted, the kinematic constrain is deactivated and the model becomes dynamically driven by slab-pull. We refer to Table 1 and our previous studies [*Baumann et al.*, 2009; *Duretz et al.*, 2011a] for details concerning the setup and physical properties of the materials involved.

[9] An evolved stage of continental collision is presented in Figure 2b. The large-scale features of our simulations are the sinking of the slab in the mantle and its interaction with the 660 km phase transition boundary that deviates the slab from its trajectory. The velocity vectors highlight the

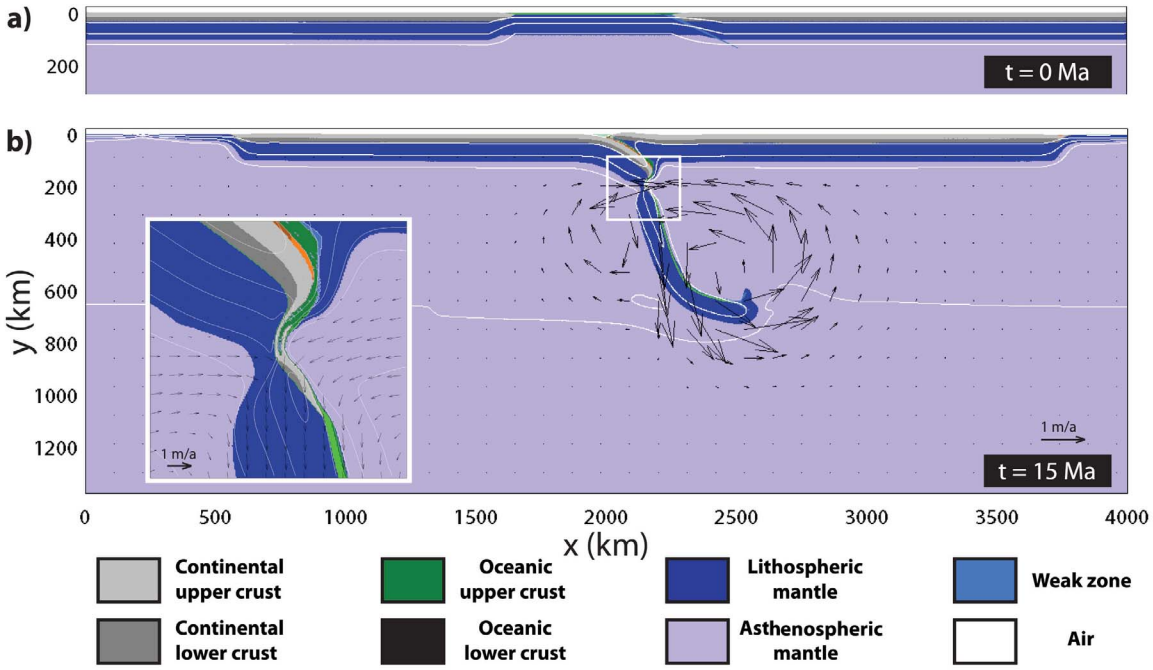

Figure 2. Representative result of the 2D thermomechanical simulations. (a) Initial setup. Initially the simulations are kinematically driven to initiate the subduction and the generation of slab pull. (b) Simulation at the stage of intermediate depth slab detachment. At this stage, the model is dynamically driven by the slab pull and the ridge push exerted by the mantle on the left and right sides of the box. The rheological parameters used in this simulation are visible in Table 1, the initial oceanic plate age is 40 Ma, the initial continental geotherm is defined using $T = 1617$ K at $z_{ADIABAT} = 140$ km and the convergence rate is 5 cm/a (applied during 10 Ma), erosion and sedimentation rates ($v_{ero} = v_{sed} = 0.1$ mm/a).

pattern of mantle flow triggered by the sinking lithospheric slab. As a consequence of the displacement of the continental plates, mantle upwelling and oceanic lithosphere generation takes place on lateral sides of the domain. The enlarged picture focuses on the location of the ongoing slab detachment and velocity arrows indicate the asthenospheric flow into the necking zone. In this simulation, the slab detachment occurs at the buried passive margin at a depth of 190 km.

3.2. The 2D Kinematics of Slab Detachment

[10] In a previous study [*Duretz et al.*, 2011a], we showed that, depending on the initial thermal age of the oceanic lithosphere and the initial convergence rate, the depth of slab detachment can range between 35 and 400 km. We also showed that, according to their depth (shallow, intermediate, deep), these detachments are affected by the activation of different deformation mechanisms within

Table 1. Physical Properties for the Different Lithologies Used in the 2D Numerical Simulations[a]

Material	k (W/m/K)	H_r (W/m^3)	C_p (J/kg)	Flow Law	η_0 (Pa^n.s)	n	E_a (J)	V_a (J/bar)	sin(ϕ)
Sediments	$0.64 + \frac{807}{T+77}$	1.50×10^{-6}	1000	wet Qz.	1.97×10^{17}	2.3	1.54×10^5	0.8	0.15
Upper cont. crust	$0.64 + \frac{807}{T+77}$	1.00×10^{-6}	1000	wet Qz.	1.97×10^{17}	2.3	1.54×10^5	0.8	0.15
Lower cont. crust	$1.18 + \frac{474}{T+77}$	0.25×10^{-6}	1000	Pl. (An75)	4.80×10^{22}	3.2	2.38×10^5	1.2	0.15
Upper oceanic crust	$0.64 + \frac{807}{T+77}$	0.25×10^{-6}	1000	wet Qz.	1.97×10^{17}	2.3	1.54×10^5	0.8	0.00
Lower oceanic crust	$1.18 + \frac{474}{T+77}$	0.25×10^{-6}	1000	Pl. (An75)	4.80×10^{22}	3.2	2.38×10^5	0.8	0.60
Mantle	$0.73 + \frac{1293}{T+77}$	2.20×10^{-8}	1000	dry Ol.	3.98×10^{16}	3.5	5.32×10^5	0.8	0.60
Weak zone	$0.73 + \frac{1293}{T+77}$	2.20×10^{-8}	1000	wet Ol.	5.01×10^{20}	4.0	4.70×10^5	0.8	0.00

[a]Qz., Pl., and Ol. correspond to the abbreviations of Quartzite, Plagioclase, and Olivine. k denotes the thermal conductivity, H_r is the radiogenic heat production, C_p is the specific heat capacity, η_0 is the reference viscosity, n is the stress exponent, E_a is the activation energy, V_a is the activation volume, ϕ is the internal friction angle. The cohesion (C) is 1 MPa for each lithology.

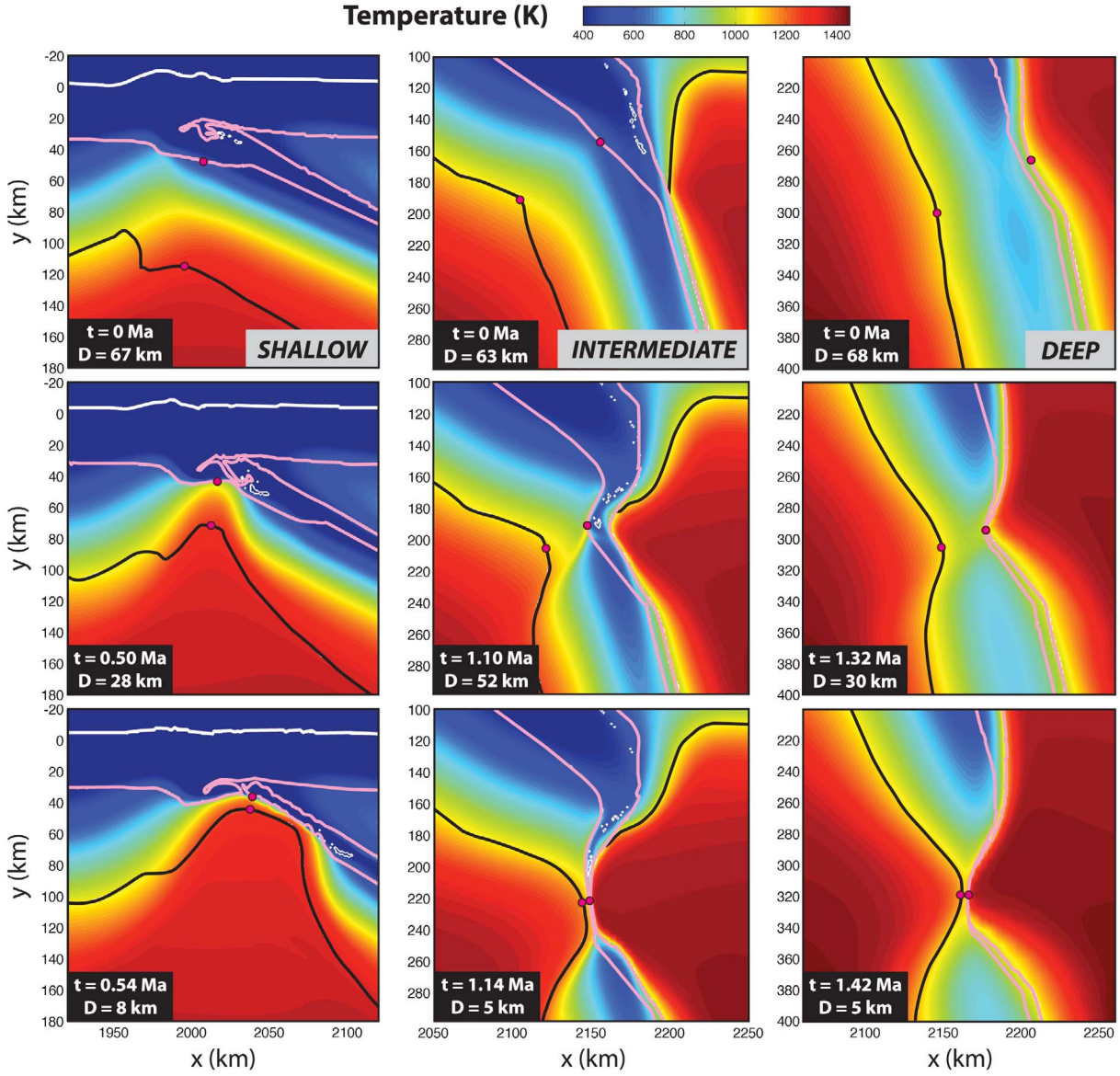

Figure 3. Thermal evolution during slab detachment at shallow, intermediate and deep depths. These three general slab detachment cases are the result of 2D thermomechanical simulations. Here, D corresponds to the slab thickness and t to the time after the onset of slab thinning. The white line defines the model surface, the pink line denotes the interface between the crust and the mantle lithosphere, and the black line denotes the lithosphere/asthenosphere boundary.

the slab. Figures 3 and 4 show the detailed temperature and viscosity field during detachment for each of the three representative cases. The color contours emphasize the location of the crust/mantle and lithosphere/asthenosphere interfaces and thus enable distinguishing the geometry of the slabs. A common characteristic of these models is that slab detachment results in distributed weakening within the thinning zone. Another common feature is the progressive weakening of the asthenosphere throughout the detachment. This shear thinning effect is the consequence of the power law deformation behavior of the asthenospheric mantle at high stress. On the other hand, according to their depth, these slab detachment models are characterized by deformation kinematics that vary from mostly pure shear (necking) to the combination of simple shear and pure shear (shear necking). These two distinct mechanisms, that eventually lead to slab detachment, are described in sections 3.3 and 3.4.

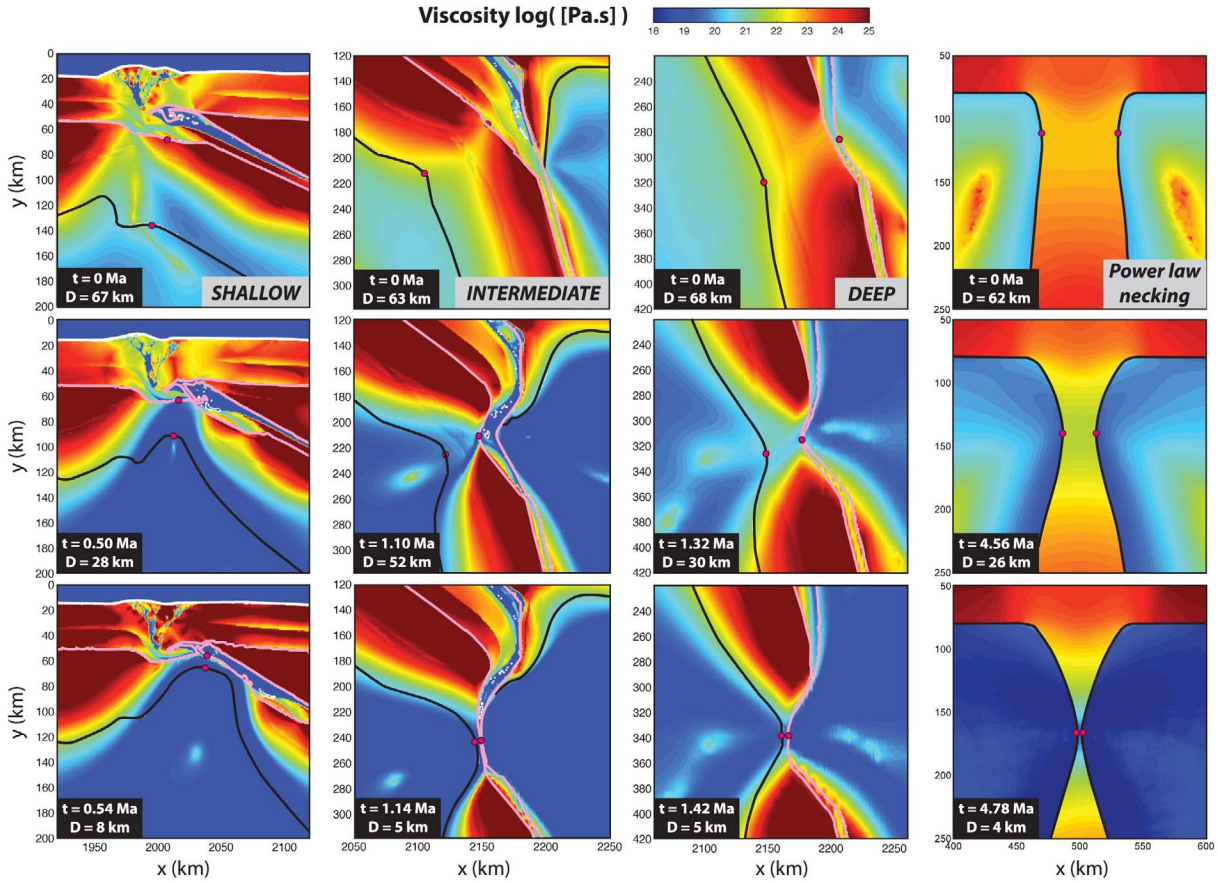

Figure 4. Evolution of the viscosity during shallow, intermediate, and deep slab detachment models. These cases are the results of large-scale thermomechanical simulations of plate collision. The white line defines the model surface, the pink line denotes the interface between the crust and the mantle lithosphere, and the black line corresponds to the lithosphere/asthenosphere boundary. The fourth column displays the viscosity evolution in a purely mechanical finite element simulation of power law necking under gravity. This simulation demonstrates the weakening pattern due to necking of a power law viscous layer (viscosity reduction in the neck) embedded in a power law viscous material (distributed weakening in the surrounding mantle).

3.3. Pure Shear Dominated Detachment: Necking

[11] The shallow and deep slab detachments both exhibit a lithospheric deformation behavior which is dominated by pure shear thinning. At shallow levels (35–100 km), slab detachment can occur as soon as two converging continental lithospheres are in contact. The thinning of the slab takes place around the passive margin and is initiated at the lower boundary of the slab. Necking occurs in a sub-horizontal direction and the slab eventually separates from the crust by gliding along the subduction shear zone. The deep detachment occurs at a depth range between 300 and 400 km and can either occur at the location of the subducted margin or within the oceanic plate. The detachment process is characterized by symmetric necking that initiates at both the upper and lower boundary of the slab. In this model, extension occurs along a sub-vertical axis, minimizing the angle to the vertical (20 to 15°). The fourth column in Figure 4 depicts the viscosity evolution of power law necking under gravity obtained from a simple 2D finite element calculation [e.g., *Schmalholz*, 2011]. This purely mechanical simulation shares the first-order features with the thermomechanical slab detachment simulations: (1) distributed weakening of the thinning slab and (2) viscosity reduction of the surrounding mantle together with ongoing necking. These morphological and rheological observations indicate the similarity between the complicated thermomechanical slab detachment process and simple necking of a power law viscous layer.

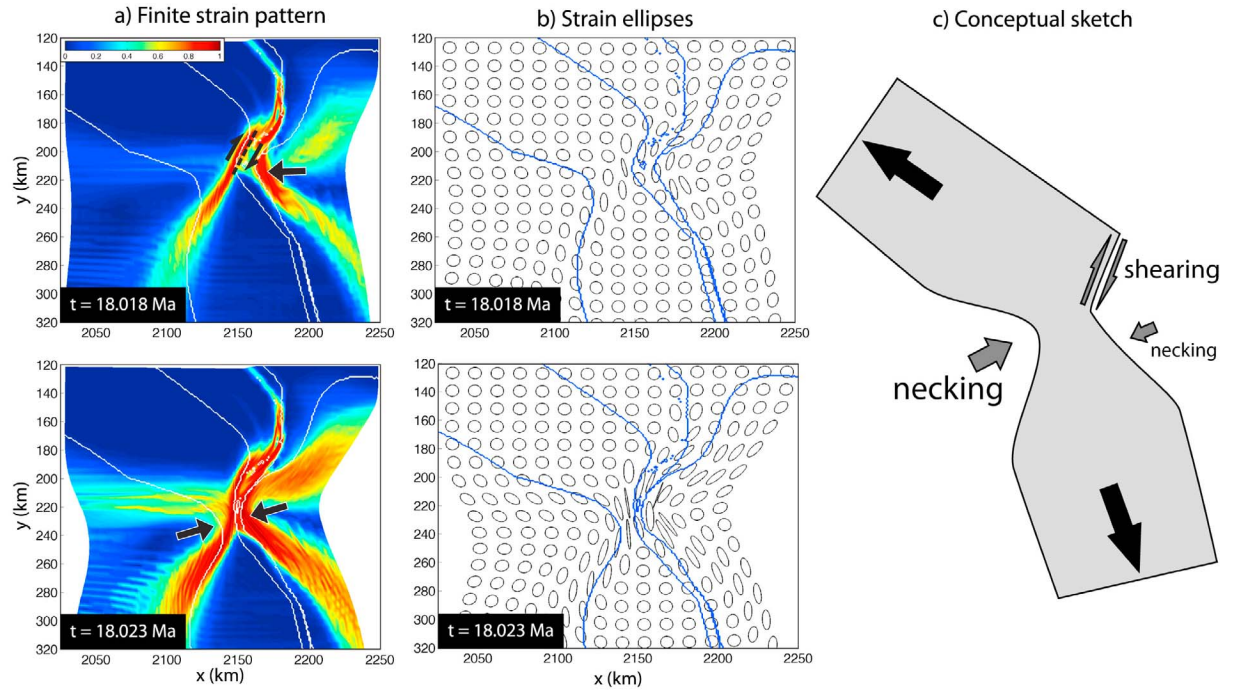

Figure 5. (a) Finite strain pattern during intermediate depth slab detachment. (top) The initial simple shear dominated regime and (bottom) the necking dominated deformation that replaces simple shear after about 30% of across slab thinning. The white lines correspond to lithological contours (crust, mantle lithosphere, asthenosphere). (b) Strain ellipses corresponding to the two stage intermediate depth slab detachment. The time frames correspond to those of Figure 5a. The blue lines correspond to the lithological contours. (c) Conceptual sketch showing the interplay of localized shear deformation in the colder parts of the slab and distributed necking in the hotter parts.

3.4. The Contribution of Pure and Simple Shear: Shearing and Necking

[12] Intermediate-depth slab detachment occurs at depths ranging between 150 and 200 km. At these depths, the continental margin that separates the buoyant continental crust from the negatively buoyant slab, enters the bending zone and start deforming. Due to its dip angle (from 35° in the continental segment to 70° in the oceanic part), the slab resides at an angle with regard to the vertical gravitational acceleration (55 to 20°). The continental margin is therefore subject to a substantial amount of simple shear deformation during the onset thinning. The first dominant feature is the development of a shear zone through the slab (Figure 5a). In the upper (colder) part of the slab, the shear zone is localized and accommodates normal-sense displacement whereas the deformation in the lower (hotter) part of the slab remains diffuse and symmetric. The transition from simple shear to pure shear thinning occurs after about 30% of across slab thinning. At this stage the shear zone starts to bend significantly and the deformation is dominated by necking. This pure shear deformation, particularly noticeable in the flattening of the strain ellipses in the core of the slab (Figure 5b), stays dominant and will eventually lead to slab detachment.

4. Comparing 2D Simulations and 1D Analytics

[13] As suggested by *Schmalholz* [2011], necking of power law viscous layers is a suitable mechanical process to explain the thinning of non-Newtonian slabs, eventually leading to their detachment. The study showed that a 1D analytical solution for viscous necking can explain the first-order dynamics of 2D necking under gravity (see Figure 4). Although this simplified pure shear necking model is valid for a homogeneous, non rheologically layered slab that vertically dips in the mantle, our 2D thermomechanical models also suggest that viscous necking can be the dominant slab-scale deformation process during slab detachment. We, therefore, compare the thinning observed in the thermomechanical 2D simulations with those predicted by

Table 2. List of the 30 Two-Dimensional Numerical Simulations of Slab Detachment and Their Differences to the Reference Run (Described in Figure 2)[a]

Run ID	Differences With the Reference Run
1 (Reference)	None
2	t_{oc} = 80 Ma, v_{conv} = 2.5 cm/a
3	t_{oc} = 20 Ma, v_{conv} = 10 cm/a
4	t_{oc} = 20 Ma, v_{conv} = 2.5 cm/a
5	t_{oc} = 20 Ma, v_{conv} = 2.5 cm/a, No Peierls
6	t_{oc} = 20 Ma, v_{conv} = 2.5 cm/a, No Peierls
7	t_{oc} = 20 Ma, v_{conv} = 2.5 cm/a, No Peierls
8	t_{oc} = 20 Ma, v_{conv} = 2.5 cm/a, No Peierls
9	v_{conv} = 2.5 cm/a
10	v_{conv} = 10 cm/a
11	t_{oc} = 30 Ma, v_{conv} = 2.5 cm/a
12	t_{oc} = 80 Ma, v_{conv} = 10 cm/a
13	t_{oc} = 80 Ma, v_{conv} = 7.5 cm/a
14	t_{oc} = 80 Ma, v_{conv} = 2.5 cm/a
15	t_{oc} = 80 Ma
16	t_{oc} = 60 Ma, v_{conv} = 7.5 cm/a
17	v_{conv} = 7.5 cm/a
18	t_{oc} = 60 Ma, v_{conv} = 2.5 cm/a
19	t_{oc} = 60 Ma
20	t_{oc} = 60 Ma, v_{conv} = 10 cm/a
21	t_{oc} = 30 Ma, v_{conv} = 7.5 cm/a
22	v_{conv} = 2.5 cm/a, $z_{ADIABAT}$ = 130 km
23	t_{oc} = 20 Ma, v_{conv} = 10 cm/a, No shear heating
24	No shear heating
25	v_{conv} = 1.25 cm/a, $z_{ADIABAT}$ = 120 km, dry olivine flow law (cont. crust)
26	v_{conv} = 1.25 cm/a, $z_{ADIABAT}$ = 120 km, dry granulite flow law (cont. crust)
27	v_{conv} = 1.25 cm/a, $z_{ADIABAT}$ = 120 km
28	v_{conv} = 1.25 cm/a, $z_{ADIABAT}$ = 120 km, plagioclase An.75 flow law (cont. crust)
29	Oceanic plate length: 700 km
30	v_{sed} = 10 cm/a

[a]The flow laws are taken from *Ranalli* [1995] and are described in Table 1.

the 1D analytical solution of slab detachment. The temporal evolution of the slab thickness was recorded in 30 2D thermomechanical numerical simulations of slab detachment (see Table 2). The simulations are chosen such that they cover a wide range of slab detachment depths. They also include detachments occurring at subducted margins and within the oceanic plate (intraoceanic). A general feature of these simulations is the occurrence of slab detachment within 15 Ma after the start of continental collision. The onset of slab detachment is here empirically defined as the moment at which the across slab strain rate yields noticeable thinning ($1 \times 10^{-15} < \dot{\epsilon}_0 < 5 \times 10^{-15}$ s^{-1}). These initially slow deformation rates are difficult to detect and the effects of variations of $\dot{\epsilon}_0$ are discussed in section 6.2. The end of slab detachment is defined by monitoring the magnitude of total slab-pull force which is defined as:

$$F_{pull} = \iint_A (\bar{\rho}_{Ast}(y) - \bar{\rho}_{Slab}(y)) g \, dx dy \quad (1)$$

where $\bar{\rho}_{Ast}$, $\bar{\rho}_{Slab}$, g and A respectively stand for the mean asthenosphere and slab density at a given depth, the acceleration of gravity and the surface area of the slab, respectively. The mean asthenosphere and slab densities are averaged horizontally (for each horizontal gridline) and the slab area is defined lithologically (upper bound is the top of the basaltic crust) and thermally (lower bound is the 1100°C isotherm). After detachment, the average density of the slab remains stable due is fast sinking velocity (high Péclet number). However, the slab/asthenosphere density contrast rapidly decreases with the increasing density of the adjacent asthenosphere. Consequently, the end of the slab detachment is related to a drop of the total slab-pull magnitude. We therefore define the detachment duration (t_{det}) as the period lasting between the beginning and the end of the detachment. Since the thickness can vary according to the initial thermal age of the lithosphere and the subduction velocity, all the thickness measurements are normalized by their initial magnitudes. Figure 6a shows the compilation of lithosphere thinning evolution for the 30 simulations. Independent of their depth, the detachment processes are characterized by a thinning acceleration with time. A second peculiarity is the fact that all detachment durations span the narrow range between 0.30 and 3.07 Ma yielding a mean detachment duration of 1.49 Ma and a median duration of 1.37 Ma with a standard deviation of 0.76 Ma. The second plot (Figure 6b) displays the same data set of slab detachment normalized by their respective detachment duration and compared to the 1D analytical solution (equation (2)). This analytical solution was derived by *Schmalholz* [2011] and has the form:

$$\frac{D}{D_0} = \left(1 - \frac{t}{t_{det}}\right)^{\frac{1}{n}} \quad (2)$$

where D/D_0 represents the slab thickness normalized by its initial thickness, t/t_{det} corresponds to the time normalized by the detachment duration. The parameter n is the characteristic stress exponent of the slab. This number describes the non-linearity that links strain rate and stress in a material with

power law viscous rheology and controls the shape of the analytical necking curve. For the space defined by the dimensionless coordinates D/D_0 and t/t_{det}, the numerical simulations of slab detachment form a narrow cluster of thinning versus time curves. These numerical results exhibit a comparable thinning evolution to that of the 1D analytical solution and the numerical models might therefore indicate that necking is the dominant process for most cases of detachment. In order to best explain our thinning data, we performed a grid search for the value of n used in the analytical solution. The results indicate that the sharpest necking curve can be described by a characteristic n = 8.48 whereas the smoothest one corresponds to a value of 2.27. A mean characteristic n = 4.13 is obtained by fitting all the necking curve and averaging the corresponding n values. This comparison shows that the 1D analytical solution with n around 4 is well suited to describe the first-order dynamics of slab detachment, i.e. the evolution of slab thickness with time around the detachment zone under buoyancy stress.

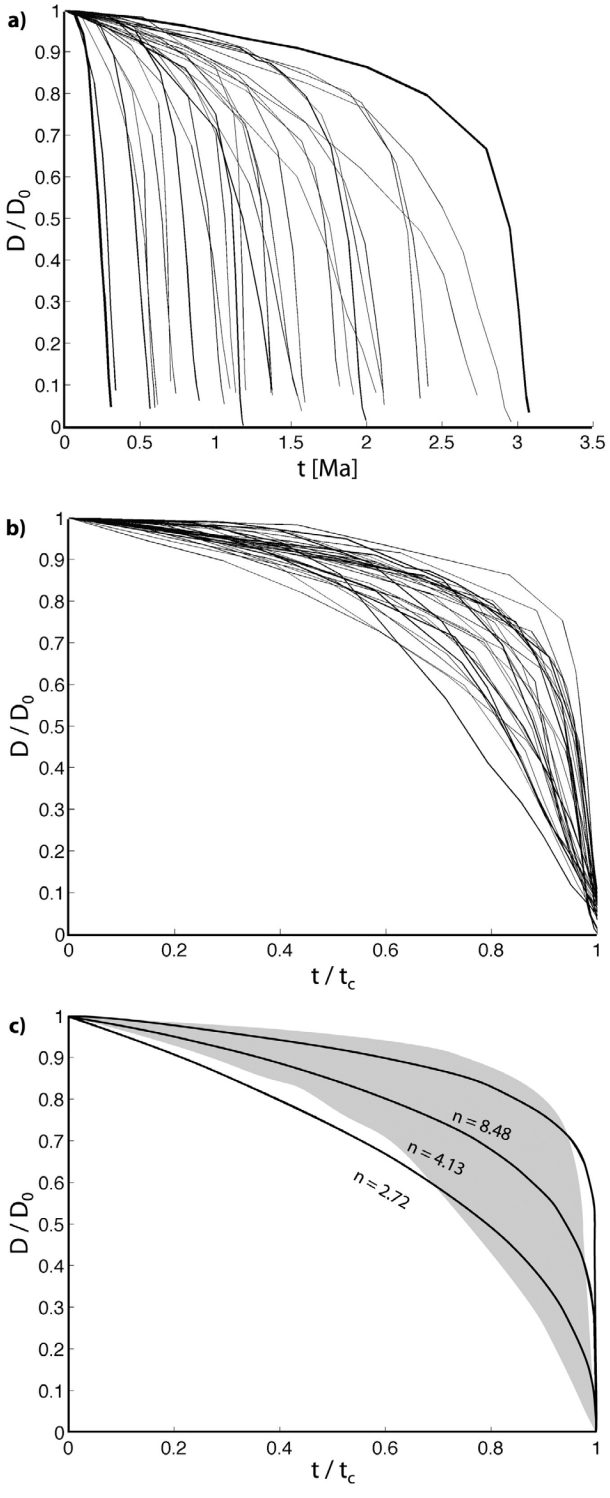

Figure 6. (a) Compilation of results of 30 2D thermomechanical simulations showing the corresponding slab thickness versus time curves. The vertical axis represents the non-dimensional slab thickness. (b) Similar plot as Figure 6a with a non-dimensional time axis. In each simulation the necking duration ($t_c = t_{det}$) defines the characteristic necking time used for the non-dimensionalization. (c) Comparison between the 1D analytical solution for necking with the thinning measured in the 2D thermomechanical simulations. The three solid lines represent the analytical solution plotted for the lowest, largest, and mean values of characteristic n calculated for our data set. The shaded area contains all the measured necking curves of the 2D simulations.

5. Impact of Shear Heating

[14] As described in section 3.2, slab detachment results from lithospheric-scale deformation involving a combination of pure and simple shearing. Since the rheology of the lithosphere is temperature-dependent, it is important to quantify the amount of mechanical energy dissipated (shear heating) during slab detachment and to understand the thermomechanical feedback on the dynamics of slab detachment. Previous 2D numerical studies [*Yoshioka et al.*, 1994; *Gerya et al.*, 2004] have investigated the role of shear heating on slab detachment by comparing simulations in which this feedback is taken into account or not. Both studies concluded that shear heating has a small influence on the deformation of the slab and can lead to an acceleration of the detachment duration. We provide here a first-order analytical result that aims

to better understand and quantify the influence of shear heating on slab detachment.

5.1. 1D Solution for Viscous Slab Necking With Shear Heating

[15] The 1D analytical solution for necking of a viscous slab due to buoyancy stress provides the evolution of the thinning factor at the zone of necking, D/D_0, with time, t [*Schmalholz*, 2011]. D is the thickness of the slab and D_0 is the initial thickness of the slab. The rate of deformation parallel to the slab, $\dot{\epsilon}$, is defined by the rate of thinning of the slab and is related to the stress, σ, by a standard power law flow law:

$$\dot{\epsilon} = -\frac{1}{D}\frac{\partial D}{\partial t} = B\,\sigma^n \tag{3}$$

[16] B is a material parameter and n is the stress exponent. Thinning is driven by the buoyancy stress and for this stress-driven necking the stress at the zone of necking is directly proportional to the thickness of the slab because the force balance along the slab requires a constant force. The product of stress times strain rate quantifies the viscous dissipation and is the shear heating source term in the equation for the evolution of the temperature, T. For simplicity, we consider here the adiabatic case with no heat conduction [*Brun and Cobbold*, 1980], which provides a maximum effect of shear heating. The material parameter B depends exponentially on temperature and this exponential dependence is described here by the Frank-Kamenetzky approximation (i.e. $B = B_0\exp(\gamma T)$). The two ordinary differential equations for the evolution of the thickness D [*Schmalholz*, 2011] and for the temperature T form a system of two coupled equations and can be written in dimensionless form:

$$\frac{\partial D}{\partial t} = -D^{1-n}\exp(T) \tag{4}$$

$$\frac{\partial T}{\partial t} = A\left(\frac{1}{D}\right)^{1+n}\exp(T) \tag{5}$$

[17] The dimensionless parameter A is:

$$A = \frac{\Delta\rho g D_0 \gamma}{2\rho c} \tag{6}$$

[18] $\Delta\rho$ is the density difference between the slab and the asthenosphere, g is the gravity acceleration, ρ is the density of the slab and c is the specific heat. The parameter $\gamma = Q/R/T_0^2$ where Q is the activation energy of the applied flow law, R is the universal gas constant and T_0 is a reference temperature [e.g., *Brun and Cobbold*, 1980; *Braeck et al.*, 2009]. The applied characteristic scales for the non-dimensionalization are:

$$D_c = D_0 \quad \text{(length)} \tag{7}$$

$$\sigma_c = \frac{1}{2}\Delta\rho g H \quad \text{(stress)} \tag{8}$$

$$t_c = \frac{1}{B\sigma_c^n} \quad \text{(time)} \tag{9}$$

$$T_c = \frac{1}{\gamma} \quad \text{(temperature)} \tag{10}$$

5.2. Application to Slab Detachment

[19] Equations (4) and (5) have been integrated numerically with explicit finite differences using a sufficiently small time step for stability and accuracy. Typical values for γ for lithospheric conditions are between 0.01 and 0.1 and typical values for A for lithospheric slabs are between 0.3 and 8. Figure 7a shows the evolution of D/D_0 with t/t_c for $A = 1.5$ and for $n = 1$ and 5. For comparison, the thinning-versus-time curves are also shown for the case of no shear heating. Shear heating decreases the duration of detachment and, as expected, accelerates necking. For $n = 1$ the duration of detachment is relatively more decreased due to shear heating than for n = 5. In the applied simple semi-analytical solution, when the thickness goes to zero the stress goes to infinity. This is impossible in nature and the stress is limited by either a plastic yield stress or a brittle failure stress. These stress limiters are ignored in the applied solution because it is used to quantify the duration of detachment. The duration of detachment does not vary considerably once the thinning versus time curve is close to vertical which happens for most parameters when values of D/D_0 are smaller than about 0.4 and stresses are therefore only moderately increased for $0.4 < D/D_0 < 1$. Figure 7b shows a contour map of the ratio of the duration of detachment without shear heating to the duration of detachment with shear heating. In other words, the numbers of the contours specify the factor that quantifies how much shorter the duration of detachment is if shear heating is considered. Shear heating shortens the time of detachment by an order of magnitude for $A > 10$. Realistic values of A for lithospheric slabs

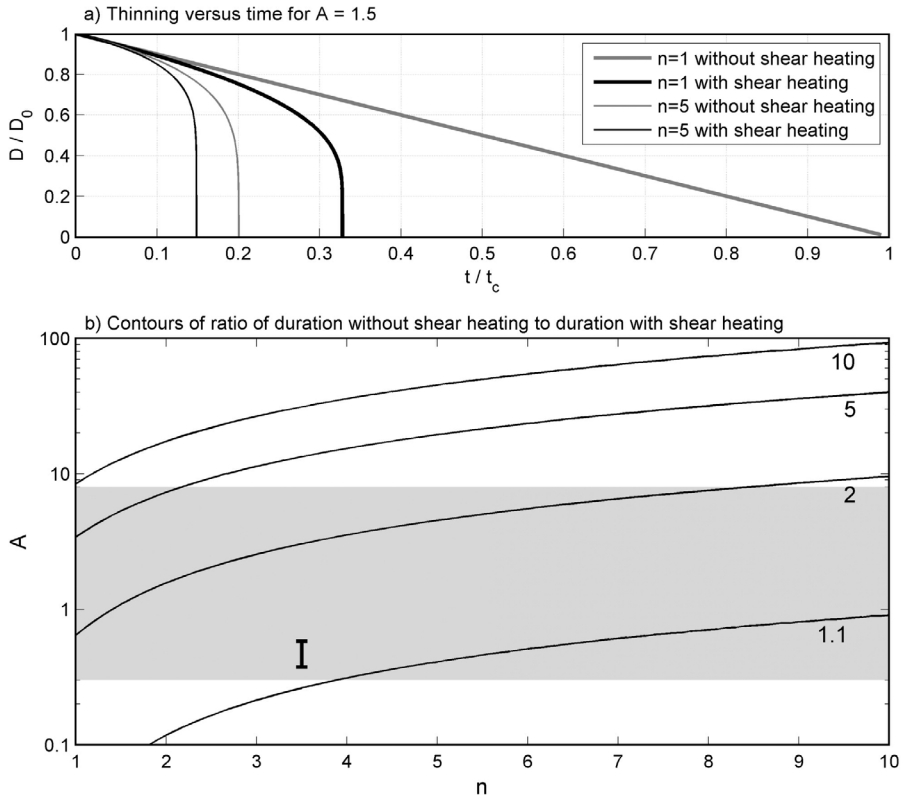

Figure 7. (a) Thinning factor, D/D_0, versus dimensionless time, t/t_c, for $A = 1.5$ and for stress exponents $n = 1$ and 5. (b) Contours for the ratio of duration of detachment without shear heating to the duration of detachment with shear heating in the space n - A. The gray shaded area indicates the realistic range of values for A expected for lithospheric slabs. The additional symbol represents the estimation of A (with $n = 3.5$) for the parameters of the simulations of *Gerya et al.* [2004].

are in the approximate range $0.3 < A < 8$ and Figure 7b indicates that for this range it is expected that shear heating shortens the duration of detachment by maximal a factor of about 5 for small n. Because heat conduction is ignored the factor of 5 is a maximum estimate and more realistic factors are expected to be smaller. For example, *Gerya et al.* [2004] predicted that slab detachment will happen 8% earlier after the start of their experiments (22.7 Ma versus 24.6 Ma) with shear heating. Using the parameters employed in the simulations of *Gerya et al.* [2004] ($n = 3.5$, $Q = 532$ kJ/mol, $R = 8.314$ J/mol/K, $c = 1000$ J/kg, $\rho = 3300$ kg/m^{-3}, $D = 80$ km), using $T_0 = 773 - 973$ K and assuming that $\Delta\rho$ is on the order of 50 kg/m^{-3}, the non-dimensional quantity A spans between 0.4 and 0.6. For such values of A the semi-analytical solution predicts detachment duration accelerations that are slightly faster than 10 % (see Figure 7b). This acceleration only applies to the detachment duration. Although this is not directly comparable to the acceleration predicted by *Gerya et al.* [2004], it is still in good agreement. Therefore, the predictions of the semi-analytical solution regarding the impact of shear heating agree well with results of 2D thermomechanical numerical simulations, if the corresponding parameters are used.

6. Discussion

6.1. Differences Between 1D Analytical and 2D Numerical Models

[20] In the simple 2D slab detachment models of *Schmalholz* [2011], it was shown that the presence of a lid (continent) can be the source of discrepancies between the 2D numerical and 1D analytical results. Although our 2D thermomechanical models reproduce the first-order dynamics of necking, it is evident that many processes are likely to affect the necking dynamics, causing the results to deviate from the 1D analytical solution. These processes induce rheological and geometrical complexities which are the major reasons that can

Table 3. Sensitivity of the Main Results for Variable Variations of the Initial Thinning Rate[a]

$\sigma_{\dot{\epsilon}_0}$ (s^{-1})	n^{min}	n^{max}	n^{mean}	t_{det}^{min} (Ma)	t_{det}^{max} (Ma)	t_{det}^{mean} (Ma)
10^{-16}	2.274 ± 0.010	8.501 ± 0.199	4.133 ± 0.008	0.304 ± 0.001	3.068 ± 0.025	1.490 ± 0.002
2.10^{-16}	2.257 ± 0.019	8.499 ± 0.421	4.140 ± 0.018	0.302 ± 0.002	3.092 ± 0.055	1.494 ± 0.006
3.10^{-16}	2.271 ± 0.028	8.783 ± 0.799	4.151 ± 0.034	0.303 ± 0.003	3.074 ± 0.077	1.496 ± 0.009
4.10^{-16}	2.265 ± 0.033	8.436 ± 0.824	4.149 ± 0.035	0.303 ± 0.004	3.212 ± 0.229	1.502 ± 0.019
5.10^{-16}	2.257 ± 0.051	8.920 ± 1.658	4.169 ± 0.052	0.302 ± 0.006	3.297 ± 0.281	1.508 ± 0.016

[a]The mean value and standard deviation of each parameter are calculated out of 20 tests of the entire data set (30 detachments). Each test consists in a pseudo-random variation (normal distribution) of the initial thinning rates $\dot{\epsilon}_0$ with a corresponding standard deviation $\sigma_{\dot{\epsilon}_0}$.

explain the difference between the simulations and the analytical results (Figure 6c). The characteristic n values obtained from fitting the 1D solution to the 2D results are therefore affected by these processes. Such deviations can result from the way slab-pull is considered in the 1D and 2D simulations. The 1D model neglects the viscous resistance of the asthenosphere and thus assumes that the entire slab-pull is involved in the slab deformation. On the other hand, numerical simulations take into account the sinking of a slab in a finite viscosity asthenosphere. This viscous resistance reduces the net effect of slab-pull [*Schellart*, 2004], therefore just a fraction of the total pull is involved in the detachment. In other words, a simulation that accounts for a partially transmitted pull can lead to underestimated values of n (<3.5) in the sense of the analytical solution. Conversely, the largest value of n = 8.48 may result from the activation of Peierls creep within the slab core [*Duretz et al.*, 2011a]. It was shown that the activation of Peierls mechanism can lead to effective stress exponents that are larger than the stress exponents for the standard power law flow law for dislocation creep in olivine [*Schmalholz and Fletcher*, 2011]. The average value of characteristic n = 4.13 is relatively close to the power law dislocation creep stress exponent of olivine.

6.2. Sensitivity of the Results

[21] The onset of slab detachment is characterized by a very slow thinning rate which complicates the exact determination of its timing in the 2D simulations. Consequently, the final results (slab detachment duration, characteristic n evaluation) depend on the criteria used to infer when detachment starts. As described in section 4, the onset of each detachment is determined by the corresponding slab thinning rate. Our 30 data curves are characterized by their initial thinning rates ($\dot{\epsilon}_0$) ranging between 1 and 5×10^{-15} s^{-1}. In order to evaluate the influence of this detachment onset criterion, we have introduced a variability of the initial thinning rate for each individual experiment. The initial strain rate is defined as: $\dot{\epsilon}_0 \approx \Delta D/D_0/\Delta t_0$. Keeping $\Delta D/D_0$ constant, a change in the initial strain rate is inversely proportional to Δt_0. Thus, variations of the initial detachment time are taken into account by perturbing the initial strain rates. These perturbations are calculated assuming a normal distribution of standard deviation ($\sigma_{\dot{\epsilon}_0}$) varying between 1×10^{-16} and 5×10^{-16} s^{-1}. A total of 100 data set perturbations were performed (20 tests for fives values of $\sigma_{\dot{\epsilon}_0}$). A maximum value of $\sigma_{\dot{\epsilon}_0} = 5 \times 10^{-16}$ s^{-1} corresponds to a variation of thinning velocity of about 1 mm/a for a 70 km thick slab. The sensitivity of the minimum, maximum, and mean values of detachment duration and characteristic n are presented in Table 3. For the maximum value of $\sigma_{\dot{\epsilon}_0}$, the mean detachment time (t_{det}^{mean}) of 1.508 ± 0.016 Ma was obtained over the 20 tests. The mean characteristic stress exponent (n^{mean}) showed more sensitivity and is equal to 4.169 ± 0.052 for the same value of $\sigma_{\dot{\epsilon}_0}$. Similarly, the other tested parameters (t_{det}^{min}, t_{det}^{max}, n^{min}, n^{max}) are also close to the values presented in the above sections.

6.3. Comparison With Previous Studies

[22] Most of the 2D thermomechanical numerical modeling studies indicated that slab detachment is the results of a progressive viscous thinning [*Yoshioka et al.*, 1994; *Schott and Schmeling*, 1998; *Gerya et al.*, 2004; *Andrews and Billen*, 2009; *Burov and Yamato*, 2008; *Baumann et al.*, 2009]. Our study yields similar results and detailed inspection of the models highlights the role of simple shearing (Figure 5c), especially at the onset of detachment when slabs detach in a moderate depth range (150–200 km). These results are comparable to the model presented by *Lister et al.* [2008] which proposes the combination of both necking and shearing processes. Concerning the duration of the detachments, our results differs from those of *Baumann et al.* [2009], leading to detachment durations that are significantly smaller (Figure 8a). This can be explained by the different

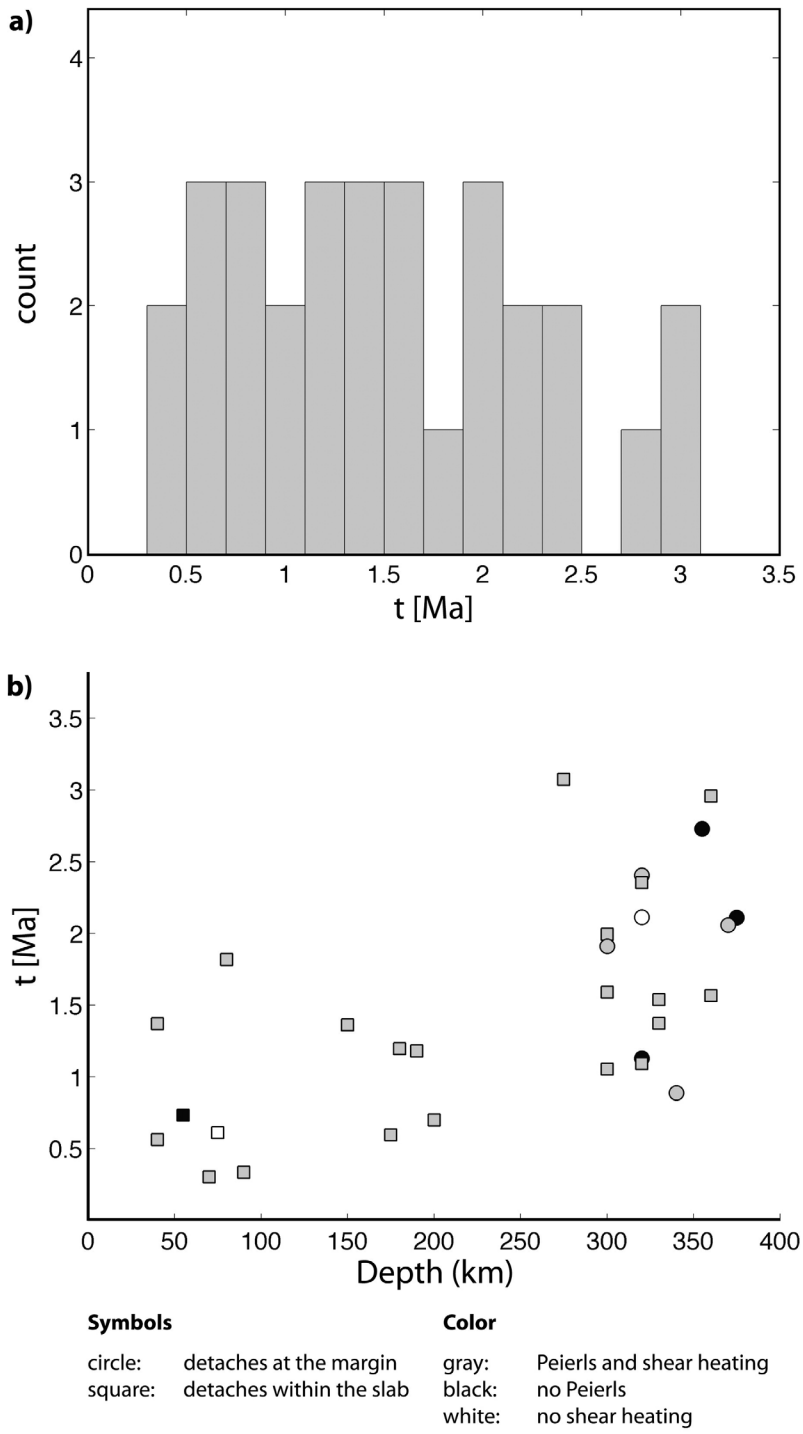

Figure 8. (a) Frequency histogram showing the range of slab detachment durations obtained in the 30 2D thermo-mechanical simulations. (b) Diagram showing the correlation between the depth of slab detachment and the duration of detachment. The different symbols contrast the simulations in which detachment occurred at different locations: either at the subducted margin or within the subducting oceanic lithosphere. The different filling colors are used to distinguish between the simulations in which both the Peierls mechanism and shear heating are activated and those in which either shear heating or Peierls mechanism is deactivated.

criteria that were used to determine the end of detachments. In this study, we have considered the dramatic decrease of slab-pull as the criterion for determining the end of the detachment periods. However, in the simulations (composition field), the slab might still be visually connected by a thin, unresolved, viscous filament. These weak filaments can remain visually attached for a long period of time but do not transfer any slab-pull to the overriding plates. Correlating the disappearance of such filaments with the end of slab detachment [*Baumann et al.*, 2009] yields to considerably longer detachment durations. Our compilation of 2D slab detachment data indicates that the necking duration is independent of depth. The relation between slab detachment duration and depth is depicted in Figure 8b. Similarly to the conclusion of *Baumann et al.* [2009], no clear correlation was observed between duration and depth of detachment since fast detachments ($t_{det} < 2$ Ma) happen in the entire considered depth range. On the other hand, slow slab detachments ($t_{det} > 2$ Ma) are only likely to occur at depths greater that 250 km. Intraoceanic (away from the margin) slab detachment (squared boxes) only occurs at large depths.

6.4. Timing of Slab Detachment, Duration and Consequences

[23] Fast detachment durations have major implications for the overlying collision zone. The inflow of asthenosphere in the detachment zone is proportional to the thinning rate of the slab. This heat advection process is expected to occur in a narrow time range (0.25–3.5 Ma) and has major consequences for the thermal structure of the orogen. The rapid loss of the slab-pull force causes a dramatic change in the force balance within orogens. Once the slab-pull force is no more transmitted to the orogen, the buoyancy of the buried continental margin may become a dominant force. According to the magnitude of the lateral forces acting on the system (e.g. ridge push), the buoyancy of the orogenic root can trigger an internal reorganization of the collision zone (eduction of *Andersen et al.* [1991]) which can cause widespread extension and might be involved in the exhumation of high-pressure rocks. Another important consequence of slab detachment is the resulting topographic response [*Buiter et al.*, 2002; *Gerya and Yuen*, 2003a]. In the work by *Duretz et al.* [2011a], a relation between slab detachment depth and surface uplift rates was highlighted. This response affects both forearc and backarc basins and can be related to the dimensions of the lithosphere deflection (induced by oceanic subduction) at the moment of slab detachment. In the case of shallow slab detachment ($z > 35$ km), no continental subduction is involved, the whole lithosphere deflection is relaxed in response to slab detachment. In the deeper slab detachment models ($z > 100$ km), continental subduction precedes slab detachment and reduces the magnitude of the deflection due to oceanic subduction. Since topographic relaxation timescales are inversely proportional to the deflection breadth [*Melosh*, 2011], shallow detachments may result in faster relaxation than deeper ones. The present study shows no relation between depth and duration of slab detachment and thus no link between detachment duration and the topographic response. Together with the technological advances and increasing precision of geochronological methods, high resolution (time) data is employed in tectonic reconstructions of collisions zones. For this purpose, it is important to take into consideration that slab detachment, and its consequences, can occur in a short timespan.

6.5. Three Dimensional Slab Detachment Dynamics

[24] Although slab detachment may involve three dimensional (3D) effects, the first 3D simulations of slab detachment [*van Hunen and Allen*, 2011; *Burkett and Billen*, 2010] provide evidence that viscous necking remains the dominant process. In some cases [*van Hunen and Allen*, 2011], the detachment may occur progressively in the along-trench direction and the detachment has the morphology of laterally variable viscous thinning. These results are in good visual agreement with the viscous necking and shear-necking models observed in the 2D simulations. The criteria used to determine the termination of detachment might be different in 3D models based on wether the slabs are actually detaching progressively in the third dimension. However, the analytical solution might, to some extent, be applicable to study slab thinning in the trench direction. The application of a 1D necking solution may thus be of interest for predicting the first-order dynamics of 3D slab detachment.

7. Conclusions

[25] The major mechanism leading to slab detachment is viscous creep, independent of the depth of slab detachment. In agreement with previous studies, we show that viscous necking is the

dominant mechanical process involved in slab detachment. Slab thinning may also benefit from the contribution of localized simple shearing in the colder parts of the subducted lithosphere.

[26] The duration of slab detachment is defined here as the time interval between the onset of slab thinning and the vanishing of the slab-pull force. The duration of slab detachment is geologically short (<4 Ma with $t_{det}^{mean} = 1.5 \pm 0.02$) which is of major importance for tectonic reconstructions and geodynamic interpretations. Since deep detachments (>250 km) can occur in a short timespan ($t_{det} < 1$ Ma), there is no simple correlation between the depth of slab detachment and its duration. Slab detachment in depths between 35 and 200 km occurs within periods shorter than 2 Ma.

[27] We use a 1D semi-analytical solution to evaluate the impact of shear heating on the duration of slab detachment. The analytical predictions regarding the impact of shear heating on slab detachment agree well with previously published results of 2D thermomechanical numerical simulations. The simple semi-analytical results and the corresponding dimensionless parameter are therefore useful to make a fast and reliable assessment regarding the impact of shear heating on the slab detachment duration.

[28] The applied 2D numerical simulations employ a rheological model that reflects the current knowledge of mantle rheology (i.e. viscoplastic considering Peierls mechanism) and the corresponding thermomechanical feedbacks. The 1D analytical solution considers only a power law flow law but describes well the first-order dynamics of slab detachment modeled with the 2D models. The combination of simple analytical models and elaborated numerical models assesses the validity of each model and leads to a better insight and understanding of the dynamics of slab detachment and its potential impact on plate tectonics.

Acknowledgments

[29] The manuscript has benefited from the fast and helpful reviews of Vlad Manea and Jeroen van Hunen. We thank Jean-Pierre Burg for the numerous motivating discussions and Benjamin Huet for providing the strain visualization tools. We thank Jeroen Smit for the office discussions. Author TD was funded by the SNF-EU research grant 20TO21-120535 (TOPO-4D).Author SMS was supported by the University of Lausanne. The numerical simulations were run on the ETH Brutus cluster.

References

Altunkaynak, Ş., and Ş. Can Genç (2004), Petrogenesis and time-progressive evolution of the Cenozoic continental volcanism in the Biga Peninsula, NW Anatolia (Turkey), *Lithos*, *102*(1–2), 316–340.

Andersen, T. B., B. Jamtveit, J. F. Dewey, and E. Swensson (1991), Subduction and eduction of continental crust: Major mechanisms during continent-continent collision and orogenic extensional collapse, a model based on the south Norwegian Caledonides, *Terra Nova*, *3*, 303–310.

Andrews, E. R., and M. I. Billen (2009), Rheologic controls on the dynamics of slab detachment, *Tectonophysics*, *464*(1–4), 60–69.

Austermann, J., Z. Ben-Avraham, P. Bird, O. Heidbach, G. Schubert, and J. M. Stock (2011), Quantifying the forces needed for the rapid change of Pacific plate motion at 6 Ma, *Earth Planet. Sci. Lett.*, *307*, 289–297.

Babist, J., M. R. Handy, M. Konrad-Schmolke, and K. Hammerschmidt (2006), Precollisional, multistage exhumation of subducted continental crust: The Sesia Zone, western Alps, *Tectonics*, *25*, TC6008, doi:10.1029/2005TC001927.

Baumann, C., T. V. Gerya, and J. A. D. Connolly (2009), Numerical modelling of sponaneous slab breakoff dynamics during continental collision, in *Advances in Interpretation of Geological Processes: Refinement of Multi-scale Data and Integration in Numerical Modelling*, edited by M. Spalla, A. M. Marotta, and G. Gosso, *Geol. Soc. Spec. Publ.*, *322*, 99–114.

Braeck, S., Y. Y. Podladchikov, and S. Medvedev (2009), Spontaneous dissipation of elastic energy by self-localizing thermal runaway, *Phys. Rev. E*, *80*, 046105.

Brun, J.-P., and P. R. Cobbold (1980), Strain heating and thermal softening in continental shear zones: A review, *J. Struct. Geol.*, *2*(1–2), 149–158.

Buiter, S. J. H., R. Govers, and M. J. R. Wortel (2002), Two-dimensional simulation of surface deformation caused by slab detachment, *Tectonophysics*, *354*(3–4), 192–210.

Burkett, E. R., and M. I. Billen (2010), Three-dimensionality of slab detachment due to ridge-trench collision: Laterally simultaneous boudinage versus tear propagation, *Geochem. Geophys. Geosyst.*, *11*, Q11012, doi:10.1029/2010GC003286.

Burov, E., and P. Yamato (2008), Continental plate collision, P-T-t-z conditions and unstable vs. stable plate dynamics: Insights from thermo-mechanical modelling, *Lithos*, *25*, 178–204.

Chatelain, J.-L., B. Guiller, and J.-P. Gratier (1993), Unfolding the subducting plate in the central New Hebrides island arc: Geometrical argument for detachment of part of the downgoing slab, *Geophys. Res. Lett.*, *20*(8), 655–658.

Chen, W.-P., and M. R. Brudzinski (2001), Evidence for a large-scale remnant of subducted lithosphere beneath Fiji, *Science*, *292*(2575), 2575–2579.

Connolly, J. A. D. (2005), Computation of phase equilibria by linear programming: A tool for geodynamic modelling and an application to subduction zone decarbonation, *Earth Planet. Sci. Lett.*, *236*, 524–541.

Davies, H. J., and F. von Blanckenburg (1995), Slab breakoff: A model of lithosphere detachment and its test in the magmatism and deformation of collisional orogens, *Earth Planet. Sci. Lett.*, *129*(1–4), 85–102.

Duretz, T., T. V. Gerya, and D. A. May (2011a), Numerical modelling of spontaneous slab breakoff and subsequent topographic response, *Tectonophysics*, *502*(1–2), 244–252.

Duretz, T., D. A. May, T. V. Gerya, and P. J. Tackley (2011b), Discretization errors and free surface stabilization in the finite difference and marker-in-cell method for applied geodynamics: A numerical study, *Geochem. Geophys. Geosyst.*, *12*, Q07004, doi:10.1029/2011GC003567.

Evans, B., and C. Goetze (1979), Temperature variation of hardness of olivine and its implication for polycristalline yield stress, *J. Geophys. Res.*, *84*, 5505–5524.

Faul, U. H., J. D. Fitz Gerald, R. J. M. Farla, R. Ahlefeldt, and I. Jackson (2011), Dislocation creep of fine-grained olivine, *J. Geophys. Res.*, *116*, B01203, doi:10.1029/2009JB007174.

Ferrari, L. (2004), Slab detachment control on mafic volcanic pulse and mantle heterogeneity in central Mexico, *Geology*, *32*, 77–80.

Gerya, T. V., and D. A. Yuen (2003a), Characteristics-based marker method with conservative finite-difference schemes for modeling geological flows with strongly variable transport properties, *Phys. Earth Planet. Inter.*, *140*(4), 293–318.

Gerya, T. V., and D. A. Yuen (2003b), Rayleigh-Taylor instabilities from hydration and melting propel "cold plumes" at subduction zones, *Earth Planet. Sci. Lett.*, *212*, 47–62.

Gerya, T. V., D. A. Yuen, and W. V. Maresch (2004), Thermomechanical modelling of slab detachment, *Earth Planet. Sci. Lett.*, *226*(1–2), 101–116.

Hildebrand, R. S., and S. A. Bowring (1999), Crustal recycling by slab failure, *Geology*, *27*(1), 11–14.

Hirth, G. (2002), Laboratory constraints on the rheology of the upper mantle, in *Plastic Deformation of Minerals and Rocks*, *Rev. in Mineral. and Geochem.*, vol. 51, edited by S. Karato and H. R. Wenk, pp. 97–120, Mineral. Soc. of Am., Washington, D. C.

Isacks, B., and P. Molnar (1969), Mantle earthquake mechanisms and the sinking of the lithosphere, *Nature*, *223*(5211), 1121–1124.

Kameyama, M., D. A. Yuen, and S.-I. Karato (1999), Thermal-mechanical effects of low-temperature plasticity (the Peierls mechanism) on the deformation of viscoelastic shear zone, *Earth Planet. Sci. Lett.*, *168*(1–2), 159–172.

Karato, S.-I. (2010), Rheology of the Earth's mantle: A historical review, *Gondwana Res.*, *18*(1), 17–45.

Katayama, I., and S.-I. Karato (2008), Rheological structure and deformation of subducted slabs in the mantle transition zone: Implications for mantle circulation and deep earthquakes, *Phys. Earth Planet. Inter.*, *168*(3–4), 125–133.

Kundu, B., and V. K. Gahalaut (2011), Slab detachment of subducted Indo-Australian plate beneath Sunda arc, Indonesia, *J. Earth Syst. Sci.*, *120*(2), 193–204.

Levin, V., N. Shapiro, J. Park, and M. Ritzwoller (2002), Seismic evidence for catastrophic slab loss beneath Kamchatka, *Nature*, *418*, 763–767.

Li, L., X. Liao, and R. Fu (2002), Slab breakoff depth: A slowdown subduction model, *Geophys. Res. Lett.*, *29*(3), 1041, doi:10.1029/2001GL013420.

Lippitsch, R., E. Kissling, and J. Ansorge (2003), Upper mantle structure beneath the Alpine orogen from high-resolution teleseismic tomography, *J. Geophys. Res.*, *108*(B8), 2376, doi:10.1029/2002JB002016.

Lister, G., B. Kennett, S. Richards, and M. Forster (2008), Boudinage of a stretching slablet implicated in earthquakes beneath the Hindu Kush, *Nature*, *1*, 196–201.

Martin, M., and F. Wenzel (2006), High-resolution teleseismic body wave tomography beneath SE-Romania—II. Imaging of a slab detachment scenario, *Geophys. J. Int.*, *164*(3), 579–595.

Melosh, H. J. (2011), *Planetary Surface Processes*, Cambridge Univ. Press, Cambridge, U. K.

Morley, C. K., and S. Back (2008), Estimating hinterland exhumation from late orogenic basin volume, NW Borneo, *J. Geol. Soc.*, *165*, 353–366.

Mugnier, J.-L., and P. Huyghe (2006), Ganges basin geometry records a pre-15 Ma isostatic rebound of Himalaya, *Geology*, *34*(6), 445–448.

Nolet, G. (2009), Slabs do not go gently, *Science*, *324*(5931), 1152–1153.

Ranalli, G. (1995), *Rheology of the Earth*, 2nd ed., Chapman and Hall, London.

Raterron, P., Y. Wu, D. J. Weidner, and J. Chen (2004), Low-temperature olivine rheology at high pressure, *Phys. Earth Planet. Inter.*, *145*, 149–159.

Replumaz, A., A. M. Negredo, S. Guillot, and A. Villasenor (2010), Multiple episodes of continental subduction during India/Asia convergence: Insight from seismic tomography and tectonic reconstruction, *Tectonophysics*, *483*(1–2), 125–134.

Rogers, R. D., H. Kárason, and R. D. van der Hilst (2002), Epeirogenic uplift above a detached slab in northern Central America, *J. Geol. Soc.*, *30*(11), 1031–1034.

Rozel, A., Y. Ricard, and D. Bercovici (2011), A thermodynamically self-consistent damage equation for grain size evolution during dynamic recrystallization, *Geophys. J. Int.*, *184*(2), 719–728.

Sacks, P. E., and D. Secor (1990), Delamination in collisional orogens, *Geology*, *18*, 999–1002.

Schellart, W. P. (2004), Quantifying the net slab pull force as a driving mechanism for plate tectonics, *Geophys. Res. Lett.*, *31*, L07611, doi:10.1029/2004GL019528.

Schmalholz, S. M. (2011), A simple analytical solution for slab detachment, *Earth Planet. Sci. Lett.*, *304*(1–2), 45–54.

Schmalholz, S. M., and R. C. Fletcher (2011), The exponential flow law applied to necking and folding of a ductile layer, *Geophys. J. Int.*, *184*(1), 83–89.

Schmandt, B., and E. Humphreys (2011), Complex subduction and small-scale convection revealed by body-wave tomography of the western United States upper mantle, *Earth Planet. Sci. Lett.*, *297*, 435–445.

Schott, B., and H. Schmeling (1998), Delamination and detachment of a lithospheric root, *Geology*, *296*, 225–247.

van der Meer, D., W. Spakman, D. van Hinsbergen, M. L. Amaru, and T. H. Torsvik (2010), Towards absolute plate motions constrained by lower-mantle slab remnants, *Nat. Geosci.*, *3*, 36–40.

van de Zedde, D. M. A., and M. J. R. Wortel (2001), Shallow slab detachment as a transient source of heat at midlithospheric depths, *Tectonics*, *20*(6), 868–882.

van Hunen, J., and M. B. Allen (2011), Continental collision and slab break-off: A comparison of 3-D numerical models with observations, *Earth Planet. Sci. Lett.*, *302*(1–2), 27–37.

Widiyantoro, S., and R. van der Hilst (1996), Structure and evolution of lithospheric slab beneath the Sunda Arc, Indonesia, *Science*, *271*, 1566–1570.

Wortel, M. J. R., and W. Spakman (1992), Structure and dynamics of subducted lithosphere in the Mediterranean region, *Proc. K. Ned. Akad. Wet. Biol. Chem. Geol. Phys. Med. Sci.*, *95*(3), 325–347.

Xu, W.-C., H.-F. Zhang, R. Parrish, N. Harris, L. Guo, and H.-L. Yuan (2010), Timing of granulite-facies metamorphism in the eastern Himalayan syntaxis and its tectonic implications, *Geology*, *485*(1–4), 231–244.

Yoshioka, S., D. A. Yuen, and T. B. Larsen (1994), Slab weakening: Mechanical and thermal-mechanical consequences for slab detachment, *Isl. Arc*, *4*, 89–103.

Zeck, H. P. (1996), Betic-Rif orogeny: Subduction of Mesozoic Tethys lithosphere under eastward drifting Iberia, slab detachment shortly before 22 Ma, and subsequent uplift and extensional tectonics, *Tectonophysics*, *254*(1–2), 1–16.

Zor, E. (2008), Tomographic evidence of slab detachment beneath eastern Turkey and the Caucasus, *Geophys. J. Int.*, *175*(3), 1273–1282.